Deep Learned Ground Penetrating Radar Subsurface Features for Robot Localization

Sathira Wickramanayake [ID]
UTS Robotics Institute
University of Technology Sydney
Sydney, Australia.
Sathira.Wickramanayake@student.uts.edu.au

Karthick Thiyagarajan [ID]
UTS Robotics Institute
University of Technology Sydney
Sydney, Australia.
Karthick.Thiyagarajan@uts.edu.au

Sarath Kodagoda [ID]
UTS Robotics Institute
University of Technology Sydney
Sydney, Australia.
Sarath.Kodagoda@uts.edu.au

Abstract—Sensors help robots perceive their environment and localize themselves. Determining a robot's location requires a range of sensing systems. Depending on accuracy criteria and navigation conditions, robot localization sensors can differ. Common sensors for robot localization include encoders, GPS, cameras, LIDARs, and IMUs. Traditional sensors are not capable enough in changing environments and uneven terrain. In this paper, we propose a method based on deep learning to use the subsurface features obtained through a Ground Penetrating Radar (GPR) to estimate the odometry of a robot. This proposed method does not rely on visual features or the distance gathered from wheel encoders. The proposed approach was evaluated on a publicly available dataset, and the evaluation results show that the proposed method can be used for robot localization without the need for odometry from wheel encoders.

Index Terms—Robot Sensing, Robot Perception, Robot Localization, Robot Learning, Ground Penetrating Radar, Pipe Robotics, Infrastructure Robotics, CMU-GPR Dataset.

I. INTRODUCTION

Ground penetrating radar (GPR) is widely utilized in a variety of subsurface inspection applications, including assessment of the lunar surface [1], underground utilities [2], roads [3], pavements [4], detection of land mines [5], as well as concrete structures [6]. GPR signals are frequently interpreted as B-scan images (also known as brightness scan images). A person manually inspects such B-Scan images to identify signatures that correspond to specific objects that are located below the surface of the scanned location [7]. As the GPR is capable of capturing features below the surface, they are less likely to change over time as a result of external factors, in contrast to other conventional robotic sensors. Therefore, GPR features have the potential to be a great form of information that can be utilised in autonomous robots for localization over a longer period of time.

Some robot localization applications cannot employ standard sensors, but they do need accurate 1D odometry. The 1D odometry measures the robot's distance from its starting location. Underground pipe robots are an example [8]. In this circumstance, it is crucial to know the robot's longitudinal position to determine where to begin the pipe examination and to locate defects. Attaching pipe robots to floating platforms prevents them from employing wheel encoders. Other robots can employ wheel encoders, however, uneven terrain could cause the wheels to slip, resulting in erroneous odometry measurements. Researchers have been experimenting with RFID sensors in settings that demand precise 1D odometry [9], [10]. However, RFID sensors must be placed in advance to employ these approaches.

There have been studies on using GPR to help navigate a ground vehicle in areas where GPS, wheel encoders, LIDARs, or cameras are insufficient or not viable [11], [12]. However, to accurately navigate using the GPR features, the environment had to be explored and mapped with the assistance of GPS beforehand. It was reported in [13] regarding another real-time GPR-based localization that uses factor graphs. However, this method still requires wheel encoder distance and IMU orientation information.

Research has been done to develop deep learning techniques that can estimate the odometry of a robot using images captured by RGB cameras without the need for wheel encoders [14], [15]. These methods identify motion between successive images by making use of the characteristics present in the images. For these methods to accurately estimate the robot's position, significant features must be present in the images. However, there are some environments that do not have any visible features or have features that are always changing, such as the interior of pipes or large bare land with a very low object density in the surrounding area.

In this paper, we present a method that uses GPR features to determine the 1D odometry of a robot in an environment that possesses changes in visual features and lacks GPS reception. The proposed method does not require the distance information that is typically obtained from a wheel encoder. The key contributions include: (a) Development of a deep learning framework that estimates the 1D odometry of the robot to be used in localization applications. This model leverages Convolutional Neural Networks (CNN) for feature extraction from GPR B-scan images and Long Short Term Memory (LSTM) networks for 1D odometry estimation; (b) Evaluation of the proposed method through a publicly available dataset; and (c) Demonstrated that the proposed method does not rely on wheel encoder accuracy; just travel direction was acquired, not distance. Wheel slip or drift doesn't impact results.
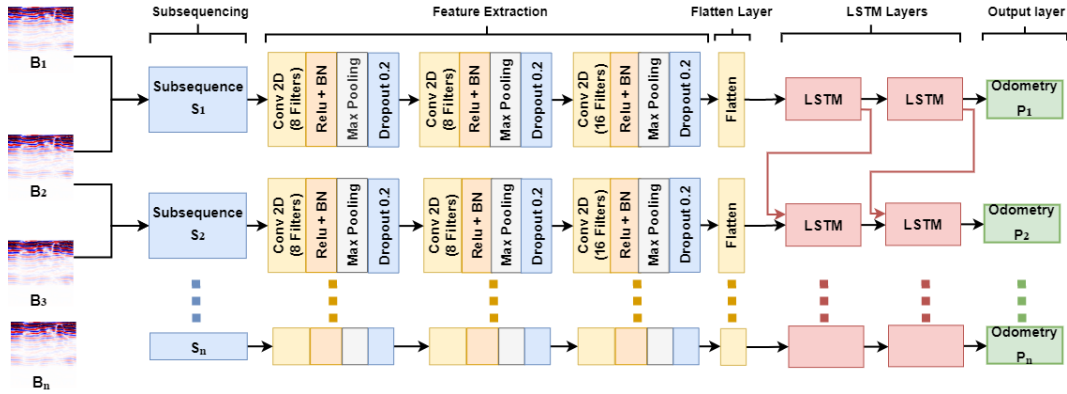
Fig. 1: The architecture of the proposed deep learning framework for robot localization is based on GPR subsurface features.

II. METHODOLOGY

A. GPR Operation and Pre-processing of GPR Data

GPR transmits radar pulses through the ground surface and receives reflections from subsurface dielectric material changes. The difference in the relative permittivities of two materials controls the reflection amplitude. Combining GPR amplitude scans (A-scans) creates B-scan images, which show GPR electromagnetic wave echoes. Subsurface objects contribute to scanned reflections. These traits can be regarded as data signatures that show up in the B-scan images in locations corresponding to those characteristics. The GPR sensor will shift these signatures across the image as the sensor moves. We can determine the robot's movements by analysing these signatures in a B-scan image. The rate of change of B-scan image features depends on the robot's speed, which can be used to calculate the robot's distance between two B-scan images. The GPR sends and receives electromagnetic waves constantly, unrelated to sensor movement. When the antenna is moved along the ground surface for a distance of X, a set of A-scans denoted as A_i ($1 \leq i \leq n$) will be gathered corresponding to the sampling frequency of the GPR antenna. Each of these A-scans will have the same length m and can be denoted as a vector of size $1 \times m$. In this work, each B-scan was produced by combining a set of 200 A-scans to form a matrix of size m x k, where $k = 200$. Given that B-scans are denoted as B_i ($1 \leq i \leq n$), each B-scan is made up of A-scans as $B_i = [A_i, A_{i+1}, A_{i+2}, ..., A_{k+(i-1)}]$.

When the robot reverses direction, the A-scan data in the B-scan images will be inverted. Hence, knowing the robot's direction is necessary. This is achieved by monitoring the tick rate of the encoder. Positive rates imply movement forwards; negative rates reverse. Since we only consider the tick rate and not the number of ticks, accurate wheel encoders are not necessary, and encoder flaws due to wheel slip will not impact the final odometry. The sensor's near-surface objects create a strong reflection in the B-scan image, hiding underlying reflections. Hence, raw B-scan images do not show subsurface features clearly. Producing B-scan images that have improved subsurface features can be accomplished through the appli-

cation of a variety of signal filtering strategies [7]. In this work, we used a Dewow filter to remove very low-frequency noise, a bandpass filter to remove high-frequency noise, and a background subtraction filter to remove the repetitive constant reflections. The background subtraction was done by calculating the sum of the A-scan signal vectors (A_i) and dividing by the number of A-scans (k) to obtain the mean A-scan vector for each B-scan, which was then subtracted from the B-scan matrix (B) to obtain the background-subtracted B-scan matrix (B_{br}). This is expressed as $B_{br} = B - [\frac{1}{k} \sum_{i=1}^{k} A_i]$. The processed B-scans are cropped and resized into images of size 128×128 to reduce the computational load during model training. The B-scan images are then combined to build pairs of consecutive B-scan images, which has a difference of 2 A-scans between them. Each pair is called a subsequence denoted as S_i ($1 \leq i \leq n$) and can be expressed as $S_i = [B_i, B_{i+2}]$. For feature extraction using 2D convolutional neural networks, we concatenate each pair of B-scans to an image with 6 channels, resulting in an input data shape of $128 \times 128 \times 6$.

B. Deep Learning Framework for Robot Localization

To extract the features in the B-scan images that correlate to the reflections created owing to the subsurface objects, a deep learning strategy that consisted of Convolutional Neural Networks (CNN) was applied. Following the 2D convolutional layers in the proposed CNN are the batch normalisation, max pooling, and dropout layers. Since the distance travelled by the robot at any point in time is dependent on its previous position, this becomes a sequence learning problem. As a result, a recurrent neural network (RNN) was required to calculate the distance travelled across the sequence of B-scan images fed into the model. Traditional RNN networks have vanishing or ballooning gradients during training [16]. This occurs when long-term dependencies are learned and grow exponentially more than their short-term counterparts. In order to predict the 1D odometry of the robot in this study, we used Long-Short-Term Memory (LSTM) networks for the regression component of the deep learning architecture. LSTMs can learn long-term dependencies and solve the vanishing gradients issue [17]. The CNN layers that are utilised for feature recognition need to
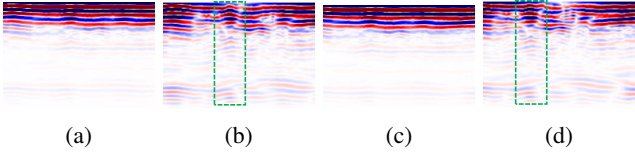
Fig. 2: Filtered images show the displacement in the sub-surface features more prominently than the unfiltered images between subsequent B-scans. The green dotted box shows the displacement of a feature between the 100th and 110th B-scan of sequence 0. (a) Unfiltered 100th B-scan image, (b) Filtered 100th B-scan image, (c) Unfiltered 110th B-scan image, and (d) Filtered 110th B-scan image.

be wrapped in time-distributed layers as this is a recurrent network. This will apply a CNN layer to every temporal B-scan image provided as an input. Following the CNN layers comes the flatten layer, which takes the multi-dimensional output from the feature extraction and turns it into a single dimension, making the data less likely to overfit. Following the two LSTM layers, which each have 1000 neurons, we added a time-distributed dense layer at the output with one neuron. Figure 1 presents the entire model architecture of the proposed deep learning framework.

III. RESULTS

The proposed deep learning framework was evaluated using a publicly available dataset (CMU-GPR Dataset) collected using a manually pulled experimental rig [18]. This rig consists of a Noggin 500 GPR, YUMO quadrature encoder with 1024 PPR, XSENS MTI-30 9-axis Inertial Measurement Unit, and an Intel RealSense D435. A Leica TS15 total station was also used to obtain the 2D ground truth location. The data from all of the sensors was time-synchronized. Multiple datasets were collected on a factory floor, a basement, and a parking garage. For this work, we used 11 datasets denoted as $Sequence\_0$ to $Sequence\_10$, where Sequences 0 to 6 were scans on a parking garage floor, and 7 to 10 were scans on a basement floor. The data was preprocessed by breaking it down into sub-sequences and filtering using the methods explained in Section II-A. The effects of filtering and how it enhances the B-scan images, enabling the displacement of the subsurface features between subsequent B-scans to be clearly observed, are illustrated in Figure 2. As this dataset was acquired indoors on a flat surface, the platform wheels did not slip, making the encoder data nearly identical to the ground truth. In most real-world robotic applications, wheel encoders accrue errors when the robot goes long distances, and the wheel loses contact, causing erroneous readings. We included stochastic odometry drift to emulate a realistic wheel encoder. Figure 3 shows a solid black line for altered wheel encoder odometry. The training and test data were selected in such a way as to provide a good balance between the scans from the parking garage and basement floor used for training and validation. The sequences used for training were 0, 2, 5, 4, 6, 8 and 10, while the sequences used for validation were 1, 3, 7 and 9. The deep

(a) Sequence 1
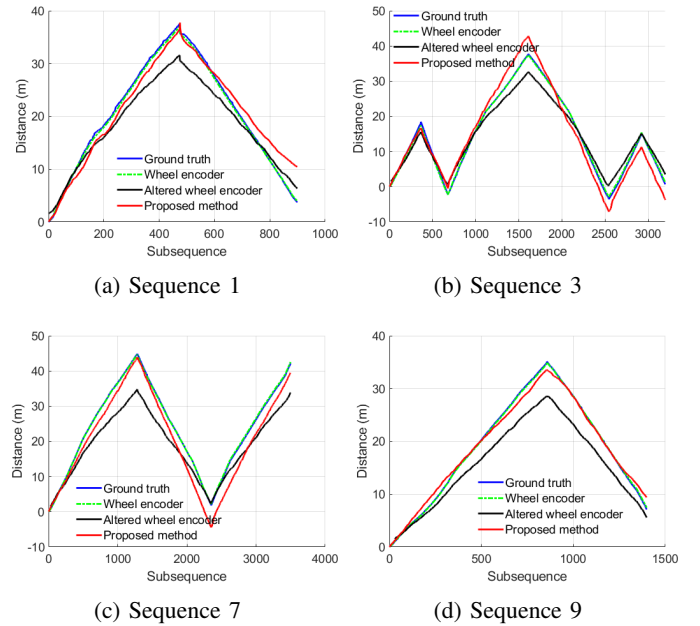

(b) Sequence 3

(c) Sequence 7

(d) Sequence 9

Fig. 3: Comparison of different odometry methods.

learning model was trained using the Adam optimizer, and a learning rate of 0.0001. The loss function used to monitor the training progress was the mean squared error (MSE), and the training was done in batches of 100 subsequences until the MSE was not further reduced. After the training process, each validation dataset was tested using the trained model. The average batch MSE of each test sequence was calculated to be 0.266, 0.403, 0.115, and 0.143 for sequences 1, 3, 7, and 9, respectively. The predicted odometry results using the proposed deep learning model are plotted against the ground truth and wheel encoder odometry for each test dataset. These results are shown in Figure 3. In all five test trajectories, the odometry was predicted reasonably well and was close to the actual odometry obtained using the wheel encoders. In all five test trajectories, the odometry estimated using the proposed method was closer to the ground truth than the altered wheel encoder data, which had wheel slip artificially introduced to mimic a realistic wheel encoding system of a robot. Therefore, the proposed method does not rely on wheel encoder accuracy; just travel direction was acquired, not distance. Wheel slip or drift doesn't impact results while using GPR.

IV. CONCLUSION AND FUTURE WORK

This paper proposes a deep learning framework for robot localization based on GPR subsurface features. Evaluations were done using an open-source dataset. The results demonstrate the proposed approach can localize a robot without encoder odometry. The proposed approach is unaffected by wheel slip in uneven terrain because it doesn't use encoder distance information. Future research will include 3D localization using GPR to determine the robot's 3D position and loop closure to improve localization accuracy. It can also be used to localize robots in pipe environments, as in [19], [20].

REFERENCES

[1] H. Song, H. Sun, J. Yang, H. Mao, M. Liu, M. Li, and X. Chen, "Diffraction separation with plane-wave destruction filer for the lunar penetrating radar sensor data," *IEEE Sensors Journal*, vol. 21, no. 22, pp. 25 198–25 205, Nov. 2021. [Online]. Available: https://doi.org/10.1109/jsen.2021.3105324

[2] S. Wickramanayake, K. Thiyagarajan, and S. Kodagoda, "Deep learning for estimating low-range concrete sub-surface boundary depths using ground penetrating radar signals," *IEEE Sensors Letters*, vol. 6, no. 3, pp. 1–4, Mar. 2022. [Online]. Available: https://doi.org/10.1109/lsens.2022.3147470

[3] Y. Wu, F. Shen, D. Xu, and R. Liu, "An ultra-wideband antenna with low dispersion for ground penetrating radar system," *IEEE Sensors Journal*, vol. 21, no. 13, pp. 15 171–15 179, Jul. 2021. [Online]. Available: https://doi.org/10.1109/jsen.2021.3068522

[4] A. Benedetto, F. Benedetto, M. D. Blasiis, and G. Giunta, "Reliability of signal processing technique for pavement damages detection and classification using ground penetrating radar," *IEEE Sensors Journal*, vol. 5, no. 3, pp. 471–480, Jun. 2005. [Online]. Available: https://doi.org/10.1109/jsen.2005.846176

[5] O. Missaoui, H. Frigui, and P. Gader, "Land-mine detection with ground-penetrating radar using multistream discrete hidden markov models," *IEEE Transactions on Geoscience and Remote Sensing*, vol. 49, no. 6, pp. 2080–2099, Jun. 2011. [Online]. Available: https://doi.org/10.1109/tgrs.2010.2090886

[6] N. Rees, K. Thiyagarajan, S. Wickramanayake, and S. Kodagoda, "Ground-penetrating radar signal characterization for non-destructive evaluation of low-range concrete sub-surface boundary conditions," *IEEE Sensors Letters*, vol. 6, no. 4, pp. 1–4, Apr. 2022. [Online]. Available: https://doi.org/10.1109/lsens.2022.3158031

[7] N. Ulapane, L. Piyathilaka, and S. Kodagoda, "Some convolution and scale transformation techniques to enhance GPR images," in *2019 14th IEEE Conference on Industrial Electronics and Applications (ICIEA)*. IEEE, Jun. 2019, pp. 1453–1458. [Online]. Available: https://doi.org/10.1109/iciea.2019.8834219

[8] A. Gunatilake, M. Galea, K. Thiyagarajan, S. Kodagoda, L. Piyathilaka, and P. Darji, "Using UHF-RFID signals for robot localization inside pipelines," in *2021 IEEE 16th Conference on Industrial Electronics and Applications (ICIEA)*. IEEE, Aug. 2021, pp. 1109–1114. [Online]. Available: https://doi.org/10.1109/iciea51954.2021.9516284

[9] A. Gunatilake, S. Kodagoda, and K. Thiyagarajan, "A novel UHF-RFID dual antenna signals combined with gaussian process and particle filter for in-pipe robot localization," *IEEE Robotics and Automation Letters*, vol. 7, no. 3, pp. 6005–6011, Jul. 2022. [Online]. Available: https://doi.org/10.1109/lra.2022.3163769

[10] A. Gunatilake, K. Thiyagarajan, and S. Kodagoda, "Evaluation of battery-free UHF-RFID sensor wireless signals for in-pipe robotic applications," in *2021 IEEE Sensors*. IEEE, Oct. 2021, pp. 1–4. [Online]. Available: https://doi.org/10.1109/sensors47087.2021.9639827

[11] T. Ort, I. Gilitschenski, and D. Rus, "Autonomous navigation in inclement weather based on a localizing ground penetrating radar," *IEEE Robotics and Automation Letters*, vol. 5, no. 2, pp. 3267–3274, Apr. 2020. [Online]. Available: https://doi.org/10.1109/lra.2020.2976310

[12] M. Cornick, J. Koechling, B. Stanley, and B. Zhang, "Localizing ground penetrating RADAR: A step toward robust autonomous ground vehicle localization," *Journal of Field Robotics*, vol. 33, no. 1, pp. 82–102, May 2015. [Online]. Available: https://doi.org/10.1002/rob.21605

[13] A. Baikovitz, P. Sodhi, M. Dille, and M. Kaess, "Ground encoding: Learned factor graph-based models for localizing ground penetrating radar," in *2021 IEEE/RSJ International Conference on Intelligent Robots and Systems (IROS)*. IEEE, Sep. 2021, pp. 5476–5483. [Online]. Available: https://doi.org/10.1109/iros51168.2021.9636764

[14] Q. Liu, H. Zhang, Y. Xu, and L. Wang, "Unsupervised deep learning-based RGB-d visual odometry," *Applied Sciences*, vol. 10, no. 16, p. 5426, Aug. 2020. [Online]. Available: https://doi.org/10.3390/app10165426

[15] S. Wang, R. Clark, H. Wen, and N. Trigoni, "DeepVO: Towards end-to-end visual odometry with deep recurrent convolutional neural networks." IEEE, may 2017, pp. 2043–2050. [Online]. Available: https://doi.org/10.1109%2Ficra.2017.7989236

[16] Y. Bengio, P. Simard, and P. Frasconi, "Learning long-term dependencies with gradient descent is difficult," *IEEE Transactions on Neural Networks*, vol. 5, no. 2, pp. 157–166, Mar. 1994. [Online]. Available: https://doi.org/10.1109/72.279181

[17] S. Hochreiter and J. Schmidhuber, "Long Short-Term Memory," *Neural Computation*, vol. 9, no. 8, pp. 1735–1780, 11 1997. [Online]. Available: https://doi.org/10.1162/neco.1997.9.8.1735

[18] A. Baikovitz, P. Sodhi, M. Dille, and M. Kaess, "Cmu-gpr dataset: Ground penetrating radar dataset for robot localization and mapping," 2021. [Online]. Available: https://arxiv.org/abs/2107.07606

[19] A. Gunatilake, L. Piyathilaka, A. Tran, V. K. Vishwanathan, K. Thiyagarajan, and S. Kodagoda, "Stereo vision combined with laser profiling for mapping of pipeline internal defects," *IEEE Sensors Journal*, vol. 21, no. 10, pp. 11 926–11 934, May 2021. [Online]. Available: https://doi.org/10.1109/jsen.2020.3040396

[20] N. Ulapane, K. Thiyagarajan, and S. Kodagoda, "Gaussian process as a benchmark for optimal sensor placement strategy," in *2021 IEEE Sensors*. IEEE, Oct. 2021, pp. 1–4. [Online]. Available: https://doi.org/10.1109/sensors47087.2021.9639873